5-2010

Higher-order eigenmodes of qPlus sensors for high resolution dynamic atomic force microscopy

Ryan C. Tung
Purdue University - Main Campus, rtung@purdue.edu

Thorsten Wutscher
Univ Regensburg

David Martinez-Martin
Univ Autonoma Madrid

R. Reifenberger
Birck Nanotechnology Center, Purdue University, reifenbr@purdue.edu

Franz Giessibl
Univ Regensburg

See next page for additional authors

Authors

Ryan C. Tung, Thorsten Wutscher, David Martinez-Martin, R. Reifenberger, Franz Giessibl, and Arvind Raman

Higher-order eigenmodes of qPlus sensors for high resolution dynamic atomic force microscopy

Ryan C. Tung,[1] Thorsten Wutscher,[2] David Martinez-Martin,[3] Ronald G. Reifenberger,[1] Franz Giessibl,[2] and Arvind Raman[1,a)]

[1]*School of Mechanical Engineering, Birck Nanotechnology Center, Purdue University, West Lafayette, Indiana 47907, USA*
[2]*Institute of Experimental and Applied Physics, University of Regensburg, 93040 Regensburg, Germany*
[3]*Departamento Fisica de la Materia Condensada, Universidad Autónoma de Madrid, 28049-Madrid, Spain*

The time response of tuning-fork based sensors can be improved by operating them at higher eigenmodes because a measurement takes at least one oscillation cycle in dynamic force microscopy and the oscillation period of the second eigenmode is only about one sixth of the fundamental mode. Here we study the higher-order eigenmodes of quartz qPlus sensors [Bettac *et al.*, Nanotechnology **20**, 264009 (2009); Giessibl and Reichling, Nanotechnology **16**, S118 (2005); Giessibl, Appl. Phys. Lett. **76**, 1470 (2000); and Giessibl, Appl. Phys. Lett. **73**, 3956 (1998)], their equivalent stiffness, and piezoelectric sensitivity, while paying special attention to the influence of the mass and rotary inertia of the sensing tip which is attached to the end of the qPlus quartz cantilever. A combination of theoretical modeling and scanning laser Doppler vibrometry is used to study the eigenmodes of qPlus sensors with tungsten tips. We find that the geometry of tungsten tips can greatly influence the shape, equivalent stiffness, and piezoelectric sensitivity of the second eigenmode of the quartz cantilever. At a critical tip length it is possible to theoretically achieve infinite equivalent stiffness and infinite piezoelectric sensitivity when the tip becomes a perfect node of vibration and beyond this critical tip length the second eigenmode loses its vibration node and the trajectory of the tip reverses with respect to the beam curvature. The findings have major implications for optimizing tip geometry for high-resolution imaging with qPlus sensors using higher eigenmodes. © *2010 American Institute of Physics*. [doi:10.1063/1.3407511]

I. INTRODUCTION

The sensing element of an atomic force microscope is key to its performance and resolution. The "qPlus sensor," a sensor built from a quartz tuning fork where one prong is fixed to some substrate and the other to which a tip is attached serves as a self-sensing cantilever,[1–4] has raised increased interest in the past years. While the first applications of qPlus showed an increased spatial resolution[5,6] and simultaneous scanning tunneling microscopy (STM) and atomic force microscopy (AFM) operation,[6,7] later applications demonstrated the capability to measure the forces that act in atomic manipulation on a piconewton scale,[8] the three-dimensional distribution of short range chemical forces on graphite,[9] surface properties of oxides,[10] the measurement of single electronic charges on single atoms,[11] and the resolving of the full structure of an organic molecule that is weakly adsorbed to a surface.[12]

While all these experiments were performed at the fundamental flexural eigenmode of the qPlus sensor, recently 300 kHz operation at the second flexural eigenmode on a modified qPlus sensor[13] was reported at Omicron Nanotechnology.[1] Thus, the qPlus sensor can also be operated in a multimode scheme[14] where the fundamental and higher eigenmodes can be excited and detected separately.

Another motivation for operation at higher flexural eigenmodes is the improved time response since at least one cycle of oscillation is needed to capture data in dynamic AFM, and the cycle time period of a second eigenmode is at least six times shorter than that of the fundamental mode. Furthermore, if a similar deflection noise density can be obtained, operation at higher frequencies results in a dramatic reduction of noise.[15]

However, in contrast to traditional silicon cantilevers, the mass and spatial extension of the tip attached at the end of a qPlus sensor cannot be neglected, in particular when higher eigenmodes are considered. The effective stiffness, piezoelectric sensitivity, as well as the sign of the tip's deflection for a given sign of the quartz beam curvature depend dramatically on the mass and moment of inertia of the tip. Here, we report on a theoretical and experimental study of the second flexural eigenmodes of qPlus sensors as a function of the tip dimensions and mass.

II. THEORETICAL MODEL

A. Fundamental and higher eigenmodes

We first begin with a theoretical model for the vibrations of the qPlus sensor to understand the influence of the geometry of the sensing tip on the fundamental and higher eigenmode properties of the quartz beam of the qPlus sensor. To analyze the vibrations of the qPlus sensor we model the

---

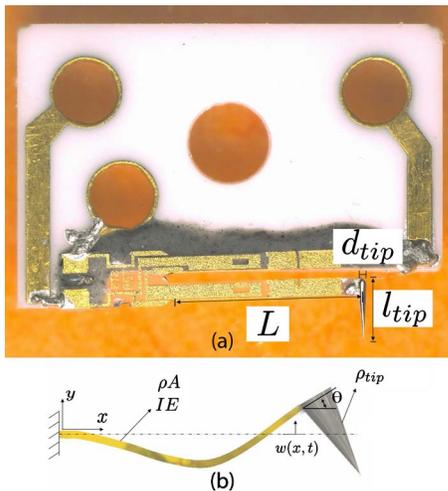a)Electronic address: raman@ecn.purdue.edu.

FIG. 1. (Color online) (a) Photograph of a qPlus sensor, (b) Mathematical model of the qPlus sensor beam and tip. L is the length of the beam, E is the Young's modulus, A is the cross sectional area of the beam, I is the area moment of the beam, ρ is the beam density, d_{tip} is the cone diameter of the tip, l_{tip} is the length of the tip, θ is the angle of the tip, and ρ_{tip} is the density of the tungsten tip.

quartz tine as an Euler–Bernoulli beam with a rigid conical tip attached at its end that possesses both transverse and rotational inertia, as depicted in Fig. 1. L is the length of the beam, E is the Young's modulus, A is the cross sectional area of the beam, I is the area moment of the beam cross section, ρ is the mass density, d_{tip} is the diameter of the base of the conical tip, l_{tip} is the length of the conical tip, and ρ_{tip} is the mass density of the tip. The geometric dimensions of a typical qPlus sensor were measured in the lab and the material properties and geometric dimensions are tabulated in Table I.

Next we express the kinetic energy, T, and the potential energy, U, of the beam-tip system as:

$$T = \frac{1}{2} \int_0^L \rho A \dot{w}^2(x,t)dx + \frac{1}{2} M_{tip} \left(\dot{w}(L,t) + \frac{d_{tip}}{2} \dot{w}_{,x}(L,t) \right)^2$$

$$+ \frac{1}{2} I_{tip} \dot{w}_{,x}^2(L,t), \tag{1a}$$

TABLE I. qPlus quartz beam and tungsten conical tip geometric and material properties used in calculations. ρ is the mass density of the beam, E is the Young's modulus of the beam, ρ_{tip} is the mass density of the tip, b is the width of the beam, h is the thickness, A is the cross sectional area of the beam, L is the length of the beam, and d_{tip} is the diameter of the base of the conical tip. Note that in the calculations the length of the tip, l_{tip}, is changed while all of the properties listed below are assumed to be constant.

qPlus material properties	
ρ (quartz)	2650 $\frac{kg}{m^3}$
E	78.7 GPa
ρ_{tip} (tungsten)	19 250 $\frac{kg}{m^3}$
b	130 μm
h	214 μm
A	27 820 μm^2
L	2.4 mm
d_{tip}	0.15 mm

$$U = \frac{1}{2} \int_0^L EIw_{,xx}^2(x,t)dx, \tag{1b}$$

where $w(x,t)$ is the transverse displacement of the beam, M_{tip} is the mass of the tip, $M_{tip} = (1/3)\pi(d_{tip}/2)^3 \rho_{tip}$, I_{tip} is the rotational inertia of the tip about the z direction calculated about the point where the base of the tip meets the end of the beam, $I_{tip} = (23/20)M_{tip}(d_{tip}/2)^2 + (1/10)M_{tip}l_{tip}^2$, over dots represent derivatives with respect to time, while $(\cdot)_{,x}$ represents a derivative with respect to x. Using Eq. (1) along with Hamilton's principle[16] we formulate equations of motion for free undamped oscillations and the relevant boundary conditions as shown below,

$$\rho A \ddot{w}(x,t) + EIw_{,xxxx}(x,t) = 0, \tag{2a}$$

$$w(0,t) = 0, \tag{2b}$$

$$w_{,x}(0,t) = 0, \tag{2c}$$

$$-M_{tip}\ddot{w}(L,t) + EIw_{,xxx}(L,t) - \frac{d_{tip}}{2}M_{tip}\ddot{w}_{,x}(L,t) = 0, \tag{2d}$$

$$I_{tip}\ddot{w}_{,x}(L,t) + EIw_{,xx}(L,t) + \frac{d_{tip}}{2}M_{tip}\ddot{w}(L,t)$$

$$+ \left(\frac{d_{tip}}{2} \right)^2 M_{tip}\ddot{w}_{,x}(L,t) = 0. \tag{2e}$$

Next assume a separable solution in the form of $w(x,t) = e^{i\omega t}\Phi(x)$, where $e^{i\omega t}$ is the temporal component of the solution, and $\Phi(x)$ is the spatial component of the solution, whose general solution is:

$$\phi(x) = C_1 \sin(\beta x) + C_2 \cos(\beta x) + C_3 \sinh(\beta x)$$

$$+ C_4 \cosh(\beta x), \tag{3}$$

where β is the nondimensional frequency defined as $\beta = (\omega^2 \rho A L^4 / EI)^{1/4}$. The boundary conditions $w(0,t) = 0$ and $w_{,x}(0,t) = 0$ give $C_2 = -C_4$ and $C_1 = -C_3$. Nondimensionalizing the preceding equations using $x = \bar{x}L$ and substituting the remaining boundary conditions from Eq. (2) into Eq. (3) we obtain a 2×2 matrix equation,

$$\begin{pmatrix} M_{11} & M_{12} \\ M_{21} & M_{22} \end{pmatrix} \begin{pmatrix} C_1 \\ C_2 \end{pmatrix} = \begin{pmatrix} 0 \\ 0 \end{pmatrix}. \tag{4}$$

The matrix $[M]$ is given by,

$$M_{11} = \beta M_{tip}[\sin(\beta) - \sinh(\beta)] + \rho AL[-\cos(\beta)$$

$$- \cosh(\beta)] + \frac{\beta^2 \frac{d_{tip}}{2}M_{tip}}{L}[\cos(\beta) - \cosh(\beta)], \tag{5}$$

$$M_{12} = \beta M_{tip}[\cos(\beta) - \cosh(\beta)] + \rho AL[\sin(\beta) - \sinh(\beta)]$$

$$+ \frac{\beta^2 \frac{d_{tip}}{2}M_{tip}}{L}[-\sin(\beta) - \sinh(\beta)], \tag{6}$$

$$M_{21} = -I_{tip}\beta^3[\cos(\beta) - \cosh(\beta)] - \rho AL^3[\sin(\beta)$$

$$+ \sinh(\beta)] + \frac{d_{tip}}{2}M_{tip}L\beta^2[\sin(\beta) - \sinh(\beta)]$$

$$- \left(\frac{d_{tip}}{2}\right)^2 M_{tip}\beta^3[\cos(\beta) - \cosh(\beta)], \qquad (7)$$

$$M_{22} = I_{tip}\beta^3[\sin(\beta) + \sinh(\beta)] - \rho AL^3[\cos(\beta) + \cosh(\beta)]$$

$$- \frac{d_{tip}}{2}M_{tip}L\beta^2[\cos(\beta) - \cosh(\beta)] - \left(\frac{d_{tip}}{2}\right)^2 M_{tip}\beta^3[$$

$$- \sin(\beta) - \sinh(\beta)]. \qquad (8)$$

For a non-trivial $\binom{C_1}{C_2}$ vector we set $\det([M]) = 0$ and solve for the countably infinite solutions for β which can be related to the natural frequencies and eigenmodes via Eq. (3). The first and second roots of this equation, and the corresponding eigenmodes, $\phi_1(x)$ and $\phi_2(x)$, are solved using the "fzero" function in MATLAB for varying tip base diameters, d_{tip}, and varying tip length, l_{tip}, for the beam/tip properties listed in Table I. Finally we scale all eigenmodes such that $\phi_i(L) = 1$ for $i = 1, 2, 3, \ldots$.[17]

Figure 2 shows the evolution of the first and second transverse eigenmodes of the system, in the case of constant tip base diameter, $d_{tip} = 0.15$ mm, and varying tip length, l_{tip}, for the beam/tip properties listed in Table I. It is clear from Fig. 2 that while the first eigenmode is barely affected by varying tip lengths the second eigenmode is substantially affected. We see that as the tip length is increased the node of the second eigenmode translates toward the end of the beam, eventually crossing the end of the beam, thus making the second eigenmode nodeless. The critical l_{tip} at which the node vanishes in this case is ≈ 0.65 mm which is within the normal range of tip lengths used with qPlus sensors, implying that this result can be easily achieved in practice. Without inclusion of tip rotational inertia the node approaches the free end of the cantilever beam only in the limit of infinite tip mass; however in the current system, the spatial extent of the tip as reflected in the rotational inertia is very important and even for reasonable finite tip mass and length it is possible for the vibration node to be situated at the sensing tip or even beyond.

Next we examine the effect that the conical tip mass has on the equivalent stiffness of the first and second eigenmode. The equivalent stiffness of a particular eigenmode is calculated by equating the strain energy of that eigenmode, $V = \frac{1}{2}\int_0^L EI[q(t)\phi_{,xx}^i(x)]^2 dx$, to the potential energy of a point-mass oscillator, $V = \frac{1}{2}k_{eq}q(t)^2$.[17] Using the nondimensional quantity $\bar{x} = x/L$, we obtain

$$k_{eq}^i = \frac{EI}{L^3}\int_0^1 [\phi_{,\bar{x}\bar{x}}^i(\bar{x})]^2 d\bar{x}, \qquad (9)$$

where k_{eq}^i is the equivalent stiffness of the ith eigenmode $\phi^i(x)$. After calculating the roots of the frequency equation k_{eq}^i is calculated analytically using Eq. (3).

Figure 3 depicts a surface plot of the equivalent stiffness of the first and second eigenmode, $k_{eq}^i = \frac{EI}{L^3}\int_0^1 [\phi_{,\bar{x}\bar{x}}^i(\bar{x})]^2 d\bar{x}$, for various tip lengths and tip base diameters, where $i = 1$ and 2
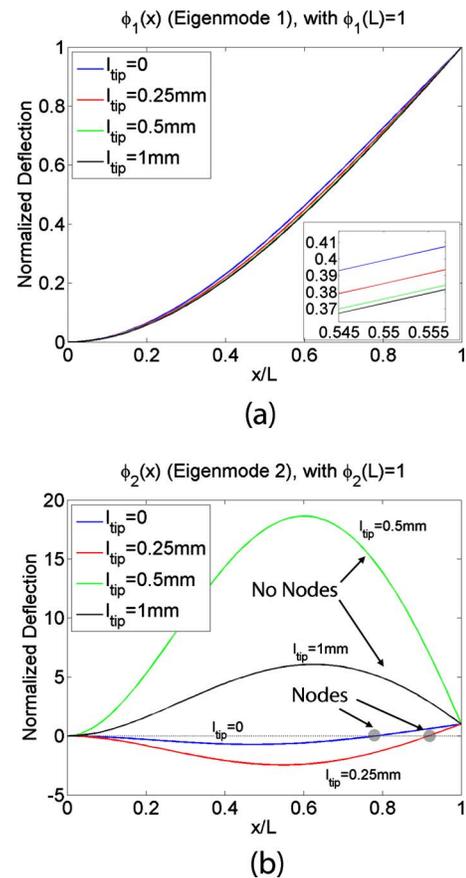

FIG. 2. (Color online) Evolution of the first and second transverse eigenmodes of the quartz beam calculated using the properties listed in Table I, for varying tip length, l_{tip}. x/L is the nondimensional position along the length of the beam. Notice that the first eigenmode is relatively unchanged, while the second eigenmode shows a drastic transformation as l_{tip} is increased. As the tip length is increased the node of the second eigenmode traverses toward $x/L = 1$, eventually crossing $x/L = 1$ effectively implying that the node of the second eigenmode vanishes. Note that the absence of nodes is a real effect, and simply reflecting the mode shape about the x axis would still show no nodes.

denote the first and second transverse eigenmodes. We see in Fig. 3(b) that for a given tip base diameter, d_{tip}, there is an optimal tip length, l_{tip}, that will achieve infinite equivalent stiffness.

At first glance this prediction is remarkable since intuition might guide us to expect an infinite equivalent stiffness for the second eigenmode only when the tip mass approaches infinity, as in Ref. 17. The current theory on the other hand suggests this singular condition can be achieved with finite tip mass. This apparent contradiction is clearly resolved by taking into account that the model also includes the rotational inertia of the tip which greatly amplifies the influence of tip inertia on the equivalent stiffness of the second eigenmode.

The fact that the stiffness of the second eigenmode can be tuned simply by tuning the size of the tungsten tip has many practical ramifications for dynamic AFM using higher eigenmodes of qPlus sensors. For example, theoretically infinite equivalent stiffness implies that the tip oscillation amplitude could be on the order of a few picometers thus providing great sensitivity to short range interaction forces. As
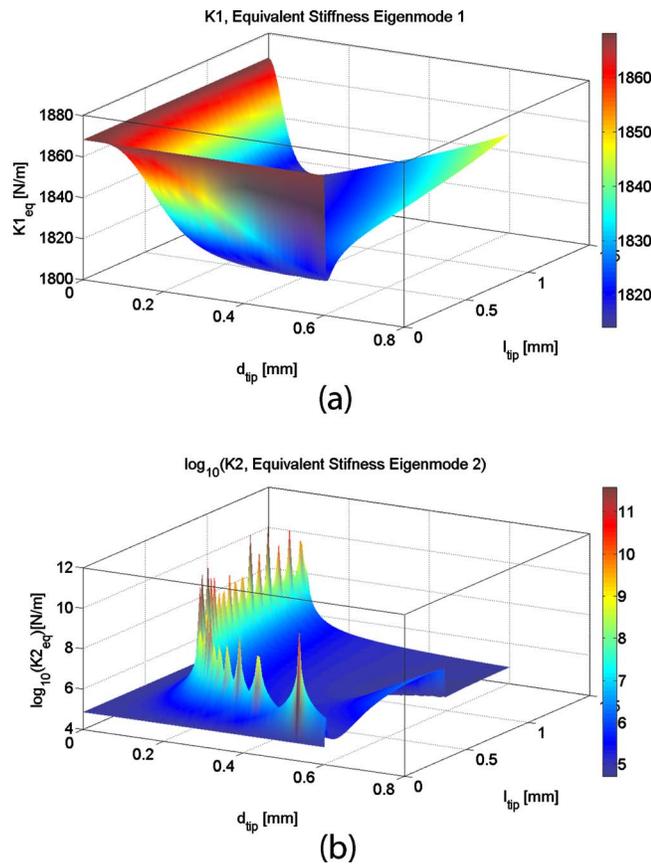
(a)

(b)

FIG. 3. (Color online) Surface plot of the equivalent stiffness of the first and second eigenmodes, $k_{eq}^i = EI/L^3 \int_0^1 [\Phi_i(\bar{x}), \bar{x}\bar{x}]^2 d\bar{x}$, for the properties listed in Table I while varying l_{tip} and d_{tip}, where $\bar{x}$ is the nondimensional distance x/L. (a) Equivalent stiffness of the first eigenmode. (b) Equivalent stiffness of the second eigenmode. Note that in (b) the peaks are numerical artifacts of the calculation grid, when the node is located at the tip position the equivalent stiffness, k_{eq}^2, is infinite.

another example, a second eigenmode without a vibration node could be desirable to ensure that the tip motion is mostly transverse without side to side motion arising from tip rotation.

B. Parasitic rotation of the tip

Ideally when excited at an eigenmode the distal end of the sensing tip should oscillate purely normal to the surface. However the quartz beam bending leads to a tip rotation which is manifest as a parasitic tip motion tangential to the surface. To understand this effect we next calculate the tip angle of the qPlus sensor while vibrating in an eigenmode with a specific transverse vibration amplitude. This is an important quantity to consider since tip rotational vibration leads to some motion of the tip tangential to the sample surface thus potentially allowing lateral forces to participate in normal force spectroscopy. Figure 1(b) depicts the maximum tip angle, θ_i, when the beam vibrates in a specific eigenmode. We calculate the angle of the tip for a unit displacement, $\phi^i(L) = 1$, by using the relation $\tan(\theta_i) = (\partial \phi^i(L)/\partial x)$. Figure 4 shows the tip angle, or the parasitic tip rotation, of the first and second eigenmodes for a unit tip displacement.
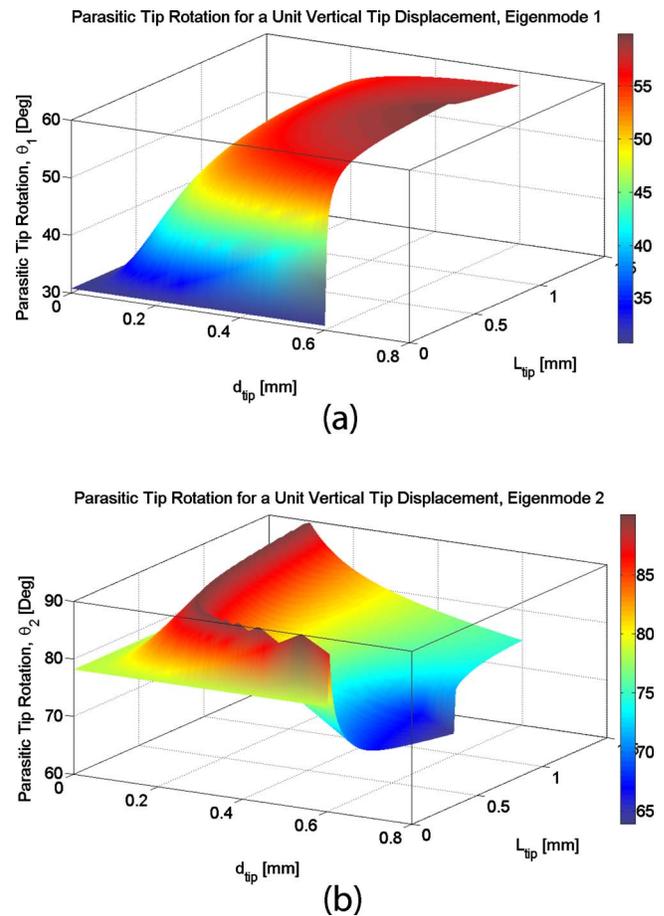

(a)

(b)

FIG. 4. (Color online) Surface plot of the angle of the tip, or parasitic tip rotation, calculated for a unit vertical tip displacement. (a) Parasitic tip rotation due to bending of the first eigenmode, for a unit vertical tip displacement. (b) Parasitic tip rotation due to bending of the second eigenmode, for a unit vertical tip displacement. Note that at the critical tip length when the tip becomes a node of vibration the tip motion is dominated by the parasitic tip rotation.

From Fig. 4 it is apparent that the tip angle is small for the first eigenmode, so long as the tip dimensions are small. The tip angle for the first eigenmode continues to increase as the dimensions of the tip are increased. The tip angle is more significant for the second eigenmode. For example, for a transverse tip motion of 1 nm (normal to the sample surface) in the second eigenmode, the lateral tip motion (tangential to the sample surface) for a tip of length, $l_{tip} \approx 0.3$ mm and $d_{tip} \approx 0.15$ mm could be as high as 4 pm. Especially when l_{tip} reaches the critical value where the tip becomes a node of vibration, the ratio of tangential to normal tip oscillation relative to the surface becomes significant.

C. Piezoelectric sensitivity

Unlike a conventional AFM probe which typically uses an optical lever setup to infer the vibration of the sensing tip, the qPlus sensor utilizes the piezoelectric effect to convert tip deflection to a measurable voltage signal. We now calculate the piezoelectric sensitivity of the qPlus sensor (volts per picometer of transverse tip motion in a given eigenmode), considering the aforementioned eigenmode analysis. The piezoelectric sensitivity is an important quantity for qPlus sen-

sor operation since it dictates the minimum tip oscillation amplitude that can be observed in experiments.

We consider the case where the only strain is the axial strain caused by bending (beam flexure) and $T_1 = ES_1 = E(-z\partial^2[w(x,t)]/\partial x^2)$, while all other stress components vanish. T_1 is the normal stress in the axial direction, S_1 is the strain in the axial direction, E is the Young's modulus, z is the distance from the neutral axis of the beam, and the electrode thickness is assumed to be negligible. The electric field in the x and y directions are assumed to be zero so that the piezoelectric constitutive relations can be written as follows:

$$S_1 = s_{11}T_1 + d_{31}E_3, \tag{10a}$$

$$D_3 = d_{31}T_1 + \epsilon_{33}E_3, \tag{10b}$$

s_{11} is the mechanical compliance in the axial direction, d_{31} is a piezoelectric coupling constant, and ϵ_{33} is a permittivity constant. Additionally from Ref. 3 we find that the electrodes on the top and bottom surface of the beam are kept at a constant and equal potential, thus $E_3 = 0$. From Eq. (10) we find:

$$D_3 = s_{11}^{-1}d_{31}S_1 = Ed_{31}\left(-z\frac{\partial^2 w(x,t)}{\partial x^2}\right). \tag{11}$$

We assume a separable solution, $w(x,t) = \phi(x)T(t)$ and integrate Eq. (11) across the width ($y = -b/2$ to $b/2$) and the length of the electrodes ($x = 0$ to L_e), which lie at the top and bottom surfaces of the beam ($z = h/2$ and $-h/2$). We note that the strain and z component of the surface normal have opposite signs, thus the charges on the top and bottom surfaces are additive. We obtain the following result for the total charge, Q, generated on the two electrodes due to unit transverse tip motion in a specific eigenmode:

$$Q = -hEd_{31}T(t)\int_0^{L_e}\int_0^b \frac{\partial^2\phi(x)}{\partial x^2}dydx. \tag{12}$$

Performing the integration of Eq. (12) and noting that $\partial\phi(0)/\partial x = 0$ for the cantilevered boundary conditions, we obtain:

$$Q = -bhEd_{31}T(t)\frac{\partial\phi(L_e)}{\partial x}. \tag{13}$$

We assume that the sensor is resonating at an eigenfrequency while operating in a specific eigenmode and let $T(t) = \cos(2\pi ft)$, using Ohm's law, $V = IR$, and the fact that $\dot{Q} = I$, we gain an expression for the piezoelectric sensitivity of the sensor. Following Ref. 3 we let $R = 100$ MΩ, $L_e = 1.6$ mm, and $d_{31} = 2.31 \times 10^{-12}$ C/N. The Young's modulus and physical parameters are given in Table I, f is the calculated eigenfrequency, $\partial\phi(L_e)/\partial x$ is obtained from the calculated eigenmode.

Figure 5 shows the calculated piezoelectric sensitivity for the first and second eigenmodes of the qPlus sensor. It is interesting that for certain values of tip length and tip base diameter the second eigenmode achieves infinite sensitivity, though as discussed earlier this is at the cost of infinite stiffness. Also, due to the electrode length, L_e, being less than the overall length beam length, L, there are combinations of tip
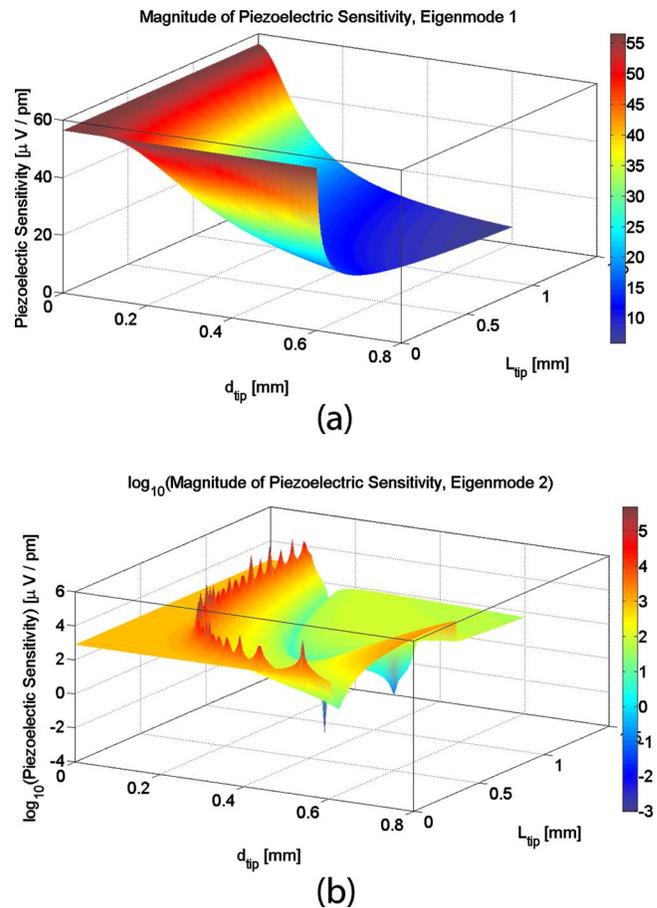

(a)

(b)

FIG. 5. (Color online) Surface plot of the piezoelectric sensitivity of the first and second eigenmodes. (a). Piezoelectric sensitivity of the first eigenmode. (b) Piezoelectric sensitivity of the second eigenmode. Note that in (b) the positive peaks are numerical artifacts of the calculation grid, when the node is located at the tip position the sensitivity is infinite. Also note that the negative peaks are also numerical artifacts of the calculation grid and the piezoelectric sensitivity of the second eigenmode becomes zero for a locus of points in parameter space.

base diameter and tip length for which the sensitivity of the second eigenmode goes to zero value, a situation which should be avoided if detection is to be performed using the piezoelectric effect of the quartz beam. The calculated piezoelectric sensitivity of the first eigenmode for $d_{tip} = 0.15$ mm and $l_{tip} \approx 0.2$ mm, which corresponds to an eigenfrequency of ≈ 28.5 kHz, agrees extremely well with a similar calculation in Ref. 3, in which the calculation was done for a static point load situated at the end of the quartz beam. This agreement can be explained by noting that the first transverse eigenmode and the deflection profile of a cantilever beam under a point load located at the free end are extremely similar, and will result in similar bending strain. It is also interesting to note that the second eigenmode displays piezoelectric sensitivities that are much larger than the first eigenmode.

In summary the results predict that tip length plays a vital role in the characteristics of the second eigenmode of the qPlus sensor. In what follows we investigate this effect experimentally. Specifically, we will study experimentally the dependence of the eigenmodes of qPlus sensors on tip geometry, the equivalent stiffnesses of the higher eigen-
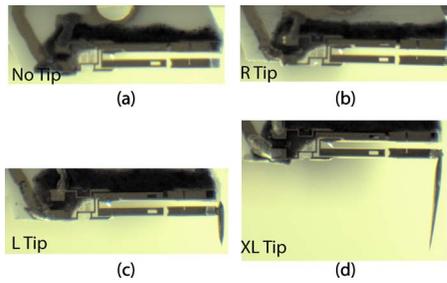
FIG. 6. (Color online) Optical images of the measured qPlus sensors. (a) No tip (No tip). (b) Regular tip (R tip). (c) Long Tip (L tip). (d) Extra long tip (XL tip).

modes and the parasitic tip rotation, while not explicitly measuring the piezoelectric sensitivity of each measured eigenmode.

III. EXPERIMENTS

The qPlus sensor is made of three parts: an alumina substrate with gold patterned electrodes, a quartz tuning fork, and a tip.[3] First, one prong of the quartz tuning fork is glued to the substrate with J-B adhesive weld.[18] The curing takes place at room temperature for 16–24 hours. Afterward a conductive two-component epoxy adhesive, Epo-Tek E 4110, is used to connect the gold patterned electrodes with the electrodes of the tuning fork.[19] The epoxy glue cures at 150 °C in 15 min. Finally, the conductive epoxy is used again to attach an etched tungsten tip.[20] This procedure was repeated to produce qPlus sensors with different tip lengths, which can be seen in Fig. 6.

Next we obtain experimental measurements of the eigenmodes of the qPlus sensors in order to validate our initial model. Note that in the following experiments we do not attempt to validate the piezoelectric sensitivity predictions via experiments. We begin by attaching the qPlus sensor to an aluminum mounting block using a nonconducting epoxy, this mounting block is attached to a piezoelectric material. The mounting is configured such that the qPlus sensor is electrically isolated from the mounting block and piezoelectric material. Figure 7 depicts a schematic of the qPlus sensor, mounting block, and piezoelectric pad.

A pseudo random excitation voltage[21] is applied to the piezoelectric material, which is an harmonic signal with randomly seeded phases and equal amplitudes in the frequency domain. The corresponding velocity signal is recorded using a scanning laser Doppler interferometer (Polytec MSA 400).[22] For each sensor 30 separate measurements are obtained at each point along the beam, and averaged in the complex domain. This yields the so-called operating deflection shapes (ODS), which for structures with small damping and widely spaced modes are equivalent to the eigenmodes. A sampling frequency of 512 kHz is used, in conjunction with a low-pass antialiasing filter and the $VD-02$ velocity decoder with a sensitivity of 125 mm/s/V.

Four qPlus sensors with various tip lengths were measured, one with no tip, one with a "regular" sized tip (denoted "R"), one with a "long" tip (denoted "L"), and one with an "extra long" tip (denoted "XL"). Figure 6 shows
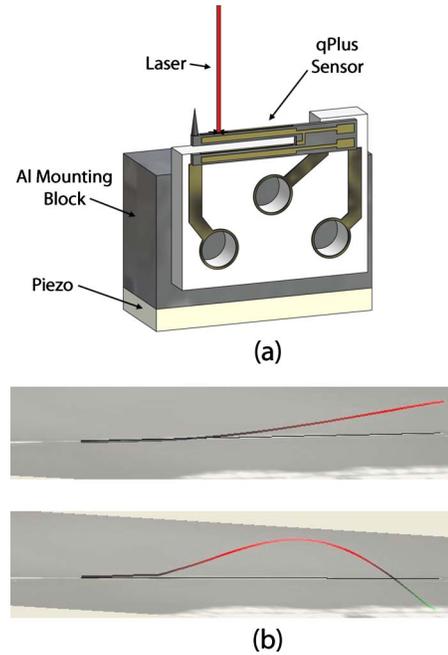

FIG. 7. (Color online) (a) Schematic depicting mounting configuration of the qPlus sensor. This set-up was used to drive and measure the transverse eigenmodes of the qPlus sensor, using the MSA 400 scanning laser Doppler interferometer. (b) Examples of experimentally measured eigenmodes of the qPlus sensor.

optical images of the aforementioned qPlus sensors. Figure 8 shows the experimental data of the measured ODSs for the first and second eigenmodes of the qPlus sensors. Table II shows the measured resonant frequencies, the experimentally calculated quality factors (Q-factors), the experimentally calculated equivalent stiffnesses and tip angles, and the ratios of the experimentally measured equivalents stiffnesses to the product of the measured Q-factors and resonant frequencies for each sensor. The Q-factors were calculated using the half power point method. The measured eigenmodes were used to evaluate the equivalent stiffness and the parasitic tip rotation.

Figure 8 clearly validates the principle of eigenmode transition that was presented in the theoretical model. In particular, the translation of the vibration node towards the distal end of the quartz beam with increasing tip length, and eventual vanishing of the node beyond a critical tip length are clearly observed. Also observed is the inversion of the sign of tip motion relative to curvature of the quartz beam when the tip length exceeds a critical value. Qualitatively there is an excellent agreement between the aforementioned theory and the experimental data with regard to the measured eigenmodes, however there are some quantitative differences. This is likely due to the simplifications used in the mathematical model. Specifically, the boundary conditions of the qPlus sensor are more complicated than the ideal case modeled here. The tip geometry was idealized as a solid cone while in experiments the tip may have voids and is clearly not an ideal right angled cone.

The equivalent stiffnesses and tip bending angles were calculated by fitting Eq. (3), obeying the geometric boundary conditions of a cantilevered beam, to the experimentally measured eigenmodes of the qPlus sensor. Next, the fit coef-
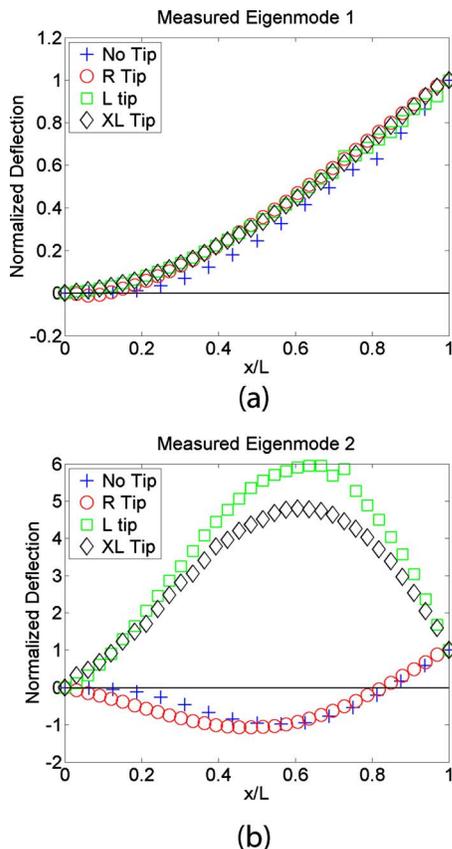
(a)

(b)

FIG. 8. (Color online) Experimentally measured ODSs of qPlus sensors. The tip displacement has been scaled to equal unity, the length has been normalized by the length of the beam. R tip denotes regular tip, L tip denotes long tip, XL tip denotes extra long tip. See Fig. 7 for photographs of the corresponding probes and tips and Tables I and II for geometrical details.

ficients and Eq. (3) were used to analytically calculate the equivalent stiffness and tip bending angle (as in Ref. 23). The results are listed in Table II. The experimentally calculated values of the equivalent stiffnesses for both eigenmodes

TABLE II. qPlus quartz beam experimentally measured quantities. l_{tip} is the approximate length of the tungsten tip of the qPlus sensor, F_i is the measured resonant frequency of the ith transverse eigenmode, Q_i is the measured Q-factor of the ith transverse eigenmode, k_{eq}^i is the experimentally calculated strain energy of the ith eigenmode, θ_i is the experimentally calculated parasitic tip rotation for unit tip transverse deflection of the ith eigenmode, k_{eq}^i/F_iQ_i, is the factor that scales the minimum detectable force gradient, i.e. the sensitivity of the probe, of the ith eigenmode ($i = 1, 2$).

qPlus sensor	No tip	R tip	L tip	XL tip
l_{tip} (mm)	0	~0.24	~0.725	~2
F_1 (kHz)	32.6	29.7	14.0	8.8
F_2 (kHz)	195.0	177.5	104.0	118.0
Q_1	3633.0	2411.1	2309.5	1091.0
Q_2	921.0	229.0	200.7	576.6
k_{eq}^1 (N/m)	2379	1890	1998	1929
k_{eq}^2 (N/m)	156.9×10^3	146.1×10^3	1981×10^3	1227×10^3
θ_1 (°)	63.2	54.2	57.6	58.1
θ_2 (°)	83.9	78.6	87.4	85.9
$\frac{k_{eq}^1}{F_1Q_1}$ (N s/m)	0.0201×10^3	0.0027×10^3	0.0618×10^3	0.2010×10^3
$\frac{k_{eq}^2}{F_2Q_2}$ (N s/m)	0.8734×10^3	3.5944×10^3	94.9106×10^3	18.0406×10^3

agree very well with the theoretically predicted values. The experimentally calculated tip angles also agree reasonably well.

With all other relevant parameters measured, it is interesting to investigate the question whether or not the tip geometry influences the force gradient sensitivity of the second eigenmode, since ultimately this is an important quantity in AFM. As given in[24,25] the minimum detectable force gradient in AFM is given by:

$$k_{min}^i = \sqrt{\frac{4k_{eq}^i k_b T B_i}{\pi F_i Q_i A_i^2}}, \tag{14}$$

where k_{eq}^i is the equivalent stiffness of the ith eigenmode, $k_b T$ is the thermal energy at the ambient temperature, B_i is the measurement bandwidth in the ith eigenmode, F_i is the ith natural frequency, Q_i is the Q-factor of the ith eigenmode, and A_i is the tip amplitude of the driven cantilever oscillation in the ith eigenmode. We can see that in Table II the ratio k_{eq}^i/F_iQ_i which is proportional to the minimum detectable force gradient is drastically affected by the tip geometry. This number increases dramatically for the second eigenmode for tip lengths near the critical length required to remove the node from that eigenmode, and then decreases for large tip lengths. This would at first sight suggest that the tip lengths near the critical value reduce the force gradient sensitivity, however, the tip amplitude in these cases is also greatly reduced which boosts sensitivity to force gradients.

IV. CONCLUSIONS

In summary, we have shown that the tip geometry and mass play a crucial role in the development of the eigenmodes of qPlus sensors. The nature of the second eigenmode can be changed significantly simply by tuning the length of the sensing tip, and it is possible to achieve infinite equivalent stiffness and piezoelectric sensitivity for reasonable tip dimensions. The high sensitivity obtainable at higher frequencies emphasizes the need for high-bandwidth preamplifiers for qPlus sensors. On the other hand tip geometries also exist that render nearly zero piezoelectric sensitivity of the second eigenmode and must be avoided. Depending on the tip dimensions, the tip motion can go from the expected case for an Euler beam with constant cross section to a case where the deflection is zero at all times and even to an inversion of the tip trajectory. This has dramatic consequences for building sensors that are optimized at the second transverse eigenmode. Short and light tips are recommended in order to keep the operation of the qPlus sensor in the second mode simple and straightforward. However, longer tips open up the possibility of unique properties but they require carefully optimized tip geometries.

[1] A. Bettac, J. Koeble, K. Winkler, B. Uder, M. Maier, and A. Feltz, Nanotechnology **20**, 264009 (2009).
[2] F. J. Giessibl and M. Reichling, Nanotechnology **16**, S118 (2005).
[3] F. J. Giessibl, Appl. Phys. Lett. **76**, 1470 (2000).
[4] F. J. Giessibl, Appl. Phys. Lett. **73**, 3956 (1998).

[5] F. J. Giessibl, S. Hembacher, H. Bielefeldt, and J. Mannhart, Science **289**, 422 (2000).

[6] S. Hembacher, F. J. Giessibl, and J. Mannhart, Science **305**, 380 (2004).

[7] S. Hembacher, F. J. Giessibl, J. Mannhart, and C. F. Quate, Phys. Rev. Lett. **94**, 056101 (2005).

[8] M. Ternes, C. P. Lutz, C. F. Hirjibehedin, F. J. Giessibl, and A. J. Heinrich, Science **319**, 1066 (2008).

[9] U. D. Schwarz, Nat. Nanotechnol. **4**, 307 (2009).

[10] G. H. Simon, T. König, M. Nilius, H.-P. Rust, M. Heyde, and H.-J. Freund, Phys. Rev. B **78**, 113401 (2008).

[11] L. Gross, F. Mohn, P. Liljeroth, J. Repp, F. J. Giessibl, and G. Meyer, Science **324**, 1428 (2009).

[12] L. Gross, F. Mohn, N. Moll, P. Liljeroth, and G. Meyer, Science **325**, 1110 (2009).

[13] M. Schmid, F. J. Giessibl, and J. Mannhart, Phys. Rev. B **77**, 045402 (2008).

[14] T. R. Rodríguez and R. Garcia, Appl. Phys. Lett. **84**, 449 (2004).

[15] F. J. Giessibl, Rev. Mod. Phys. **75**, 949 (2003).

[16] L. Meirovitch, *Principles and Techniques of Vibrations* (Prentice Hall, Upper Saddle River, NJ, 1997).

[17] J. Melcher, S. Hu, and A. Raman, Appl. Phys. Lett. **91**, 053101 (2007).

[18] *J-B WELD Company*, P.O. Box 483, Sulphur Springs, TX 75483 (2009).

[19] *POLYTEC PT*, Polytec-Platz 1–7, 76337 Waldbronn (2009).

[20] I. Ekvall, E. Wahlstrom, D. Claesson, H. Olin, and E. Olsson, Meas. Sci. Technol. **10**, 11 (1999).

[21] P. Polytec, Inc., Midwest Office 3915 Research Park Dr., Suite A-12 Ann Arbor, MI 48108, *Software Manual Polytec Scanning Vibrometer Software 8.1* (2008).

[22] P. Polytec, Inc., Midwest Office 3915 Research Park Dr., Suite A-12 Ann Arbor, MI 48108, *Hardware Manual Micro System Analyzer MSA 400* (2008).

[23] D. Kiracofe and A. Raman, J. Appl. Phys. **107**, 033506 (2010).

[24] Y. Martin, C. Williams, and H. K. Wickramasinghe, J. Appl. Phys. **61**, 4723 (1987).

[25] T. R. Albrecht, D. Grutter, D. Horne, and D. Rugar, J. Appl. Phys. **69**, 668 (1991).